Aerospace Science and Technology 26 (2013) 235–243

Contents lists available at SciVerse ScienceDirect

Aerospace Science and Technology

www.elsevier.com/locate/aescte

Performance of microstrip antenna arrays installed on aircraft

Marcos V.T. Heckler [a,*], Achim Dreher [b]

[a] Universidade Federal do Pampa, Campus Alegrete, 97546-550 Alegrete, RS, Brazil
[b] German Aerospace Center, Institute of Communications and Navigation, Oberpfaffenhofen, 82234 Wessling, Germany

ARTICLE INFO

Article history:
Received 7 January 2011
Received in revised form 29 April 2011
Accepted 8 May 2012
Available online 23 May 2012

Keywords:
Installed performance assessment
On-board antennas
Microstrip antenna arrays
IPAS project

ABSTRACT

This paper presents simulations and measurements of microstrip antenna arrays installed on civil aircraft. The main purpose is to develop a procedure to simulate microstrip arrays installed on electrically large airplanes and to validate the numerical predictions of the installed performance with measurements using scaled mock-ups. All electromagnetic analyses are done using commercial software. Design and development of the antennas used for validation and particulars regarding the simulations are presented. Comparisons between simulations and measurements of installed performance are discussed in detail.

1. Introduction

The assessment of the installed performance of antennas mounted on aircraft is a very difficult task. Some radiation patterns can be measured by performing in-flight tests, which are very expensive and allow in general the determination of only few cuts [12]. In a typical setup, there is a ground station that transmits or receives the signals to/from the antenna installed on the aircraft [14]. While the aircraft is flying, an equipment is used to store the flight data such as geographic coordinates, altitude and speed. In the post processing, these values must be processed to obtain the final radiation patterns. The main advantage of flight trials is that the tests can be made under real conditions of operation. However, such measurements are not practicable for the case of microstrip antenna arrays especially if they are installed on the top of the fuselage, since the high directivity of the array demands extremely precise maneuvers for the main beam to be pointed correctly to the ground station. Moreover, it might be difficult to scan the beam down to the location of the ground station.

Another way to assess installed performance is down scaling the dimensions of both the aircraft and the antenna, whilst scaling up the frequency for the measurements, so that all the electrical dimensions (in wavelengths) are kept the same. In such tests, a mock-up of the real aircraft and a scaled antenna model are necessary [15,3–5,11,9,10,13]. The antenna does not need to have exactly the same geometry and architecture as the full-scale one, but the radiation characteristics of the original antenna should be well represented by its scaled version. One drawback of using mock-ups is that the tolerances inherent to the fabrication process may become a critical issue, especially if the frequency considered for the measurements, which is determined by the operating frequency of the real antenna and the scaling factor of the mock-ups, must be very high. Moreover, not all details of the real aircraft can be reproduced in its scaled version. Furthermore, not all the electrical parameters are precisely known for the real aircraft and for the mock-up, such as conductivity of the airplane surface.

Alternatively to the aforementioned procedures, computer modeling can be used. The main advantage of using simulations for this purpose is the reduction of time and costs. Moreover, some electromagnetic characteristics, such as surface current densities on the aircraft surface, cannot be measured directly, but they can be calculated using appropriate computer models. The process of trying to find the optimal position to install an antenna on a given airframe is also much faster and cheaper by means of simulations than it is by experiments.

In general, modeling and experiments of installed performance are achieved only for simple radiators, such as monopole and blade antennas. Modern systems are designed employing microstrip antennas for satellite-based communication and navigation. Such antennas are attractive in the aerospace sector due to their low aerodynamic profile. The assessment of installed performance of microstrip antenna arrays with digital beamforming capabilities has not been discussed in the literature yet. Therefore, the development of a procedure to simulate microstrip antenna arrays installed on electrically large airplanes is the main focus of this paper. Validation of the numerical predictions of installed performance is achieved by comparing computations and measurements of two scaled models of aircraft for civil aviation.

* Corresponding author. Tel.: +55 55 3421 8400.
E-mail addresses: Marcos.Heckler@unipampa.edu.br (M.V.T. Heckler), Achim.Dreher@dlr.de (A. Dreher).

1270-9638/$ – see front matter
http://dx.doi.org/10.1016/j.ast.2012.05.002

The details regarding the antennas used in this work are presented in the next section. Then, the preparation of the models for the installed performance analyses and the details about the measurement setup are discussed. Finally, comparisons between simulations and measurements are shown and discussed.

2. Defeatured models of microstrip antennas

The assessment of installed performance may become computational expensive, if the electrical dimensions of the aircraft are large. Therefore, using today's computational resources, it might be necessary to approximate the characteristics of the antenna instead of including its exact model in the electromagnetic simulations. This can be called defeatured antenna model. The degree of the required defeaturing depends on the complexity of the antenna. In the case of thin monopoles, for example, their geometry does not need to be strongly defeatured. The monopoles themselves can be accurately modeled by discretizing them in straight (one-dimensional) segments. One of the concerns is how accurate the feed mechanism should be modeled. The simplest way is by means of using a delta-gap generator, which is set up in the segment of the monopole that connects it to the aircraft. A more sophisticated way is to consider a coaxial extension going inside the airframe. The monopole is fed by means of a coaxial-mode waveguide excitation. This allows modeling the transition between the coaxial connector and the outer medium rigorously.

If the antenna and the scatterer (in the present case the aircraft surface) are composed of perfect conducting material, then the integral equation to be solved needs to consider only the electric field tangential to the metallic surfaces. This is the so-called electric field integral equation (EFIE). However, more complex antennas may contain dielectrics in their structure. In the case of microstrip antennas, the inclusion of dielectric layers makes the computation time and memory needs increase rapidly with the antenna size. This effect occurs because both the electric and magnetic field components tangential to the surface of the dielectric have to be included in the calculations. Therefore, the main challenge is to try to find the best way to model the microstrip antenna on the aircraft. Firstly, it might be possible to fully model one single antenna element integrated on a fuselage, since the antenna electrical dimensions are not large. However, even for single elements printed on multilayer dielectrics, the computations may become impractical with the computation power available today.

The inclusion of a complete description of the antenna becomes even more complicated if the radiator is an array with electrical dimensions that are larger than for a single element. To the authors' knowledge, there are no references available in the open literature that deal with the detailed analysis of installed performance of microstrip antennas on airplanes.

The modeling of dielectric parts mounted on large structures demands very high computational effort. Due to this reason, it is currently impossible to include all the geometrical details of the microstrip array for an electromagnetic analysis considering the whole airframe. In [6], the authors removed a part of the aircraft surrounding the antenna and analyzed it separately. However, such a procedure results in sharp edges in the model, which introduce additional diffractions that do not exist in reality. Another approach is to use the measured radiation patterns of each array to start the computations. This procedure includes the effect of tolerances in the antenna fabrication that influences the accuracy of the final predictions. This point is especially critical for the determination of the cross-polarization component.

One possibility for the analysis of arrays is to compute the near-fields separately and use them to start the complete simulation in a further step. However, if the frequency chosen for the measurements with the mock-ups is very high, it may be difficult to obtain the predicted performance in the experiments due to the tolerances in the fabrication of the installed microstrip antenna if not even availability of antenna functionality and measurement equipment for extremely high frequencies are missing. This might be especially critical for the prediction of the cross-polarization. Moreover, the measurement of the near-fields very close to the antenna at very high frequencies may be challenging.

Another approach is to use measured far-fields to start the computations, since they are much easier to determine experimentally than the near-fields are. The main limitation of this approach is that the metallic parts of the fuselage should not be very close to the antenna. Otherwise, the accuracy of the installed performance analyses may be degraded.

3. Antennas used in the installed performance analyses

Smart antennas have the ability of scanning the main beam electronically. For this purpose, appropriate circuitry for the signal processing is needed. If scaled measurements with such antennas have to be done, the hardware must operate at the up-scaled frequency.[1] The redesign of the frontends for operation at this higher frequency may be an expensive or even an impractical solution. Moreover, the electronic circuitry may need space that is incompatible with the dimensions of a scaled mock-up. A defeatured version of this electronically steerable array is a simpler antenna presenting fixed radiation pattern. As a consequence, one fixed feeding network must be designed for each desired beamforming condition (radiation pattern). In the experiments conducted in this work, two antenna arrays with fixed feeding network have been designed: one to point the main lobe to the boresight (called here as BD array) and the other to 40° from this direction (SB array).

Two scaled mock-ups were available for our validations. The scale factors of the available airframes were given before this study has been started, since the mock-ups were already fabricated. The scale factors of both airplane are as follows: 1/15th for a Fokker 100 model and 1/18th version of an aircraft that will be called here IPAS-1 (in reference to the IPAS project, where these activities have been performed at). The shape of this last one is closely related to short range airplanes that are currently in use by commercial passenger airlines.

The antenna arrays were designed for optimum operation at 22 GHz. Equivalent frequencies for full-scale operation are 1.222 GHz for the IPAS-1 model and 1.467 GHz for the Fokker 100 aircraft. For the former mock-up, the full-scale frequency is within the L2-band (1215–1237 MHz) of the Global Positioning System (GPS) and is interesting for the analysis of installed antenna arrays for precise navigation under safety-of-life requirements [7]. For the latter, the full-scale frequency is located at the beginning of the band of *WorldSpace* satellite radio system (1467–1492 MHz). Such analysis is important to consider the performance of antennas for communication purposes.

To start the design of the arrays, the circularly polarized single element has been developed to achieve good impedance matching and axial ratio at 22 GHz. The cross-sectional view is sketched in Fig. 1(a), where the thicknesses of the top and bottom substrates of RT/duroid 5880 are 0.787 mm and 0.254 mm, respectively, with a 38 μm thick glue layer (FV6700) in-between. The single element consists of a slot-coupled square microstrip antenna with two truncated corners, as it is schematically shown in Fig. 1(b). It is excited by a microstrip line located below the ground plane. The feed line is composed of two sections of different characteristic impedances, which are realized by suitable line widths. These have been optimized in order to achieve good impedance matching.

[1] The up-scaled frequency is obtained by multiplying the real frequency (full-scale) by the scale factor of the mock-up.

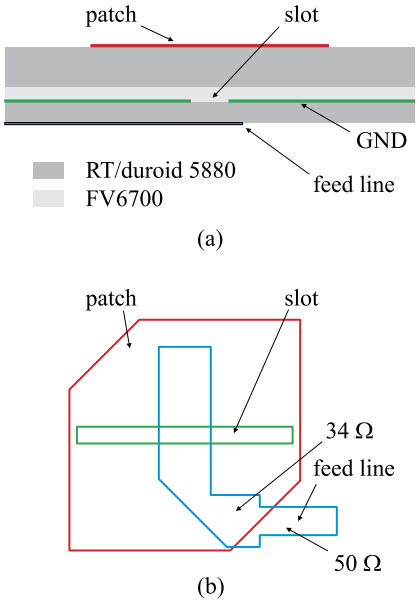

Fig. 1. (a) Cross-sectional view of a single element; (b) Schematic top view of a single element.

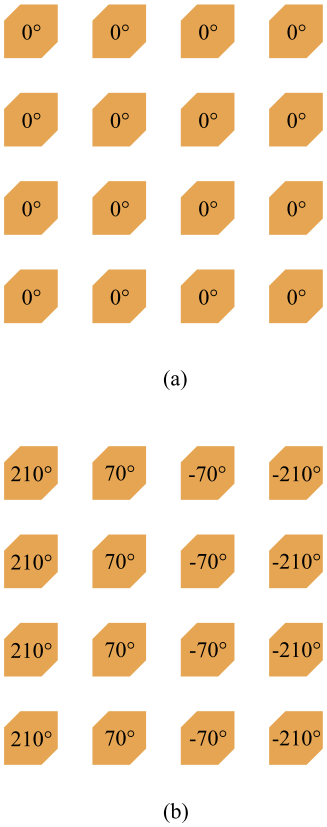

Fig. 2. Optimum phases at the input of each element. (a) Broadside array; (b) array with the main beam pointed 40° from boresight.

The number of elements in the array has been specified to 16. These are arranged in a 4×4 configuration with an inter-element spacing of $0.5\lambda_0$ at 22 GHz, which corresponds to a physical distance of 6.82 mm. This is identical for both BD and SB arrays.

For the BD array, the amplitudes and phases of the current at the input of each of the 16 elements are the same, as sketched in Fig. 2(a), whereas a relative phase shift of 140° between adjacent elements along the steering direction is necessary for the SB array, as shown in Fig. 2(b).

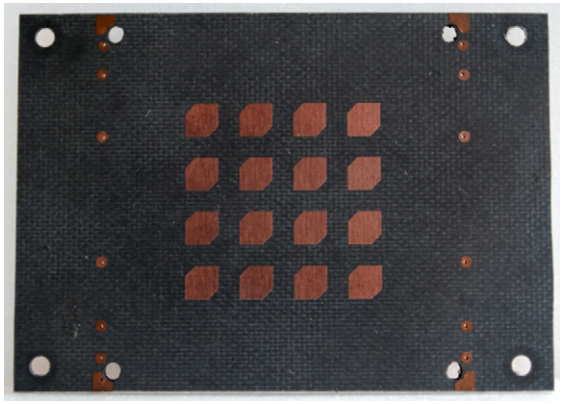

Fig. 3. Top view of the 4×4 arrays.

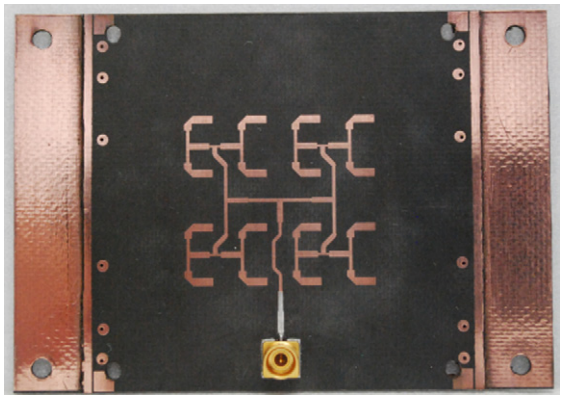

Fig. 4. Feed network of the BD arrays.

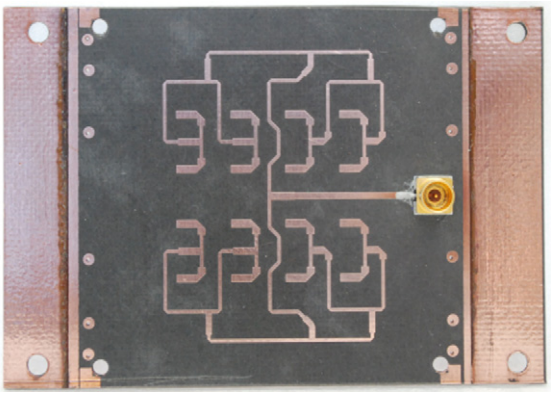

Fig. 5. Feed network of the SB arrays.

The feed network of the BD array was designed so that all the lengths of the lines are the same starting from the connector to each element. This ensures that all the elements are fed with the same phase. In the case of the SB arrays, the lines have different lengths in such a way that the elements in a row present the same phase, whereas the ones along a line (i.e. along the horizontal direction) are fed with phases showing a 140-degree phase shift.

Since tolerances in the fabrication process are critical for antennas designed to operate at 22 GHz, 5 prototypes of each array have been manufactured. Among them, one of each version of the arrays has been selected. Photos of the prototypes are shown in Figs. 3–5. The top layer with the patches (Fig. 3) is identical for both BD and SB arrays.

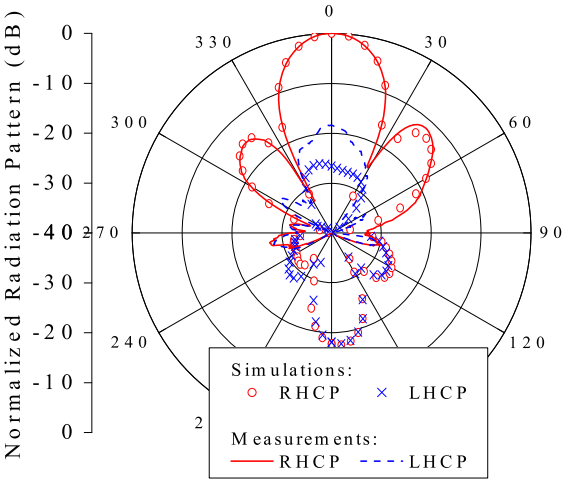

Fig. 6. Radiation pattern of the array pointing to boresight (BD array).

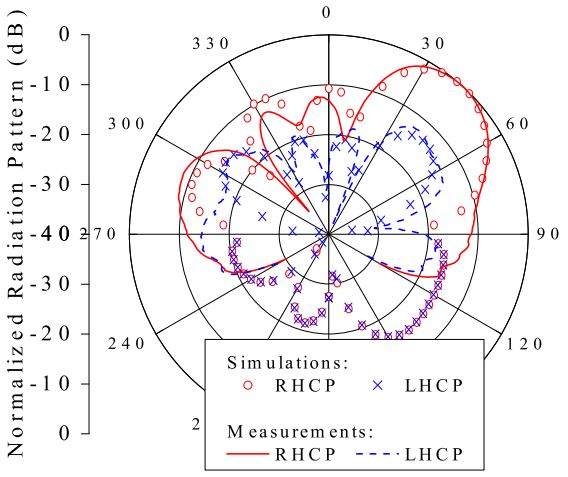

Fig. 7. Radiation pattern of the array pointing to 40° from boresight (SB array).

Figs. 6 and 7 present comparisons between the simulated and the measured radiation patterns. The simulations were performed with Ansoft Designer [1] under the assumption of infinite dielectric layers and ground planes. The measurements have been carried out in a compensated compact test range. Due to the need of using absorbers to minimize possible reflections coming from the pedestal, the patterns could not have been measured in the angular range of $120° < \theta < 240°$. Some discrepancies between both results can be observed, especially for the cross-polarization of the BD array. These are attributed to the tolerances inherent to the fabrication process, as well as to deviations in the thicknesses and dielectric constants from the nominal values given by the manufacturers of the employed laminates.

4. Description of the simulation environment for the installed performance analyses

Before starting the electromagnetic analyses, it is important to look at the electrical dimensions of the scaled mock-ups. Tables 1 and 2 present the physical and the electrical dimensions of the airframes at 22 GHz. The figures show that the models are electrically very large and this plays a very important role on the decision of which numerical technique should be used. For instance, the application of the conventional method of moments (MoM) would be too computational expensive and time consuming for the present analyses, and, therefore, will not be considered here.

Table 1
Physical and electrical dimensions (at 22 GHz) of the Fokker 100 scaled model.

	Physical dimension (mm)	Electrical dimension (λ_0)
Diameter of the fuselage	220	16.13
Total length	2350	172.33
Wingspan	1870	137.26

Table 2
Physical and electrical dimensions (at 22 GHz) of the IPAS-1 model.

	Physical dimension (mm)	Electrical dimension (λ_0)
Diameter of the fuselage	240	17.60
Total length	1693	124.15
Wingspan	1808	132.59

The electromagnetic simulator used in this study was the FEKO package [8]. In FEKO, two techniques that are suitable for the present case are physical optics (PO) and multi-level fast multipole method (MLFMM). In the former, only single reflections have been considered in our computations, whereas all multiple reflections are rigorously taken into account in the latter. Since the meshed model of the Fokker 100 formed a closed body, the MLFMM was used applying the combined field integral equation (CFIE) method. This allowed a faster solution in comparison to the electric field integral equation (EFIE) approach.

The use of the unified theory of diffraction (UTD) is also suited for very large models. However, the aircraft must be approximated by a construction made of canonical bodies only. In [16], the use of UTD for a meshed airframe has been demonstrated, but, to the authors' knowledge, this software is not available commercially yet.

With both the numerical techniques that have been selected, the airframes must be discretized prior to the analyses. The mesh generation is a very important step in the installed performance analyses, since the quality of the generated mesh has direct influence on the accuracy and on the speed of the computations. However, preparatory to the mesh generation, it is essential to obtain a cleaned[2] CAD model, since its quality influences directly the final mesh.

From the experience gained in past studies [9,10], most of the Fokker 100 airframe has been discretized considering an edge size of $\lambda_0/5$. This criterion has proven to be acceptable because the surface current density induced on the airframe is expected to be very weak and vary very slowly in the regions away from the antenna location, if the airframe is electrically large. The discretization was finer only in the tail. This resulted in a mesh of 792,118 surface triangular elements.

For the simulations with the IPAS-1 model, only a fixed mesh was available (no cleaned CAD model) so that there was no flexibility to define the edge size of the mesh elements, which was approximately $\lambda_0/8$ at 22 GHz. This resulted in a mesh of 1,388,784 surface triangular elements. Due to the large number of elements, only computations using PO have been successfully performed. Simulations with the MLFMM technique demanded computational resources exceeding the available capabilities.

[2] A cleaned model describes accurately enough the geometry of the aircraft using as less surfaces as possible. Moreover, the contact between the individual surfaces must be also guaranteed to ensure that adjacent mesh elements are electrically connected to each other.

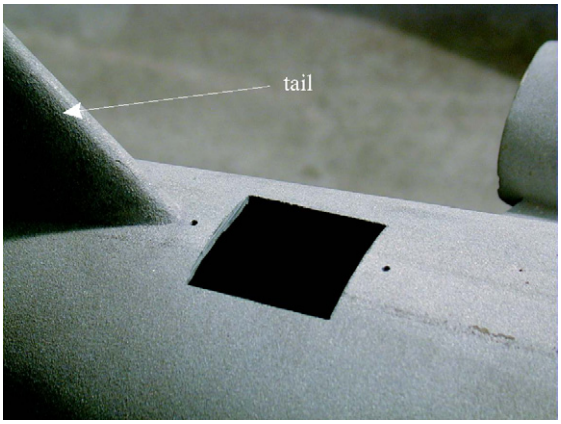

Fig. 8. Detail of the hole cut into the Fokker 100 model to accommodate the arrays.

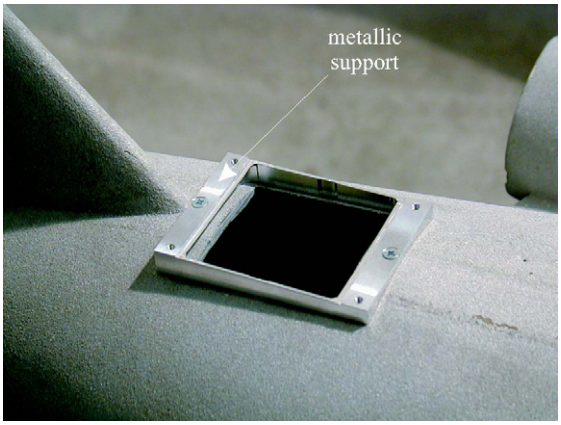

Fig. 9. Detail of the metallic support to attach the arrays on the surface of the Fokker 100 model.

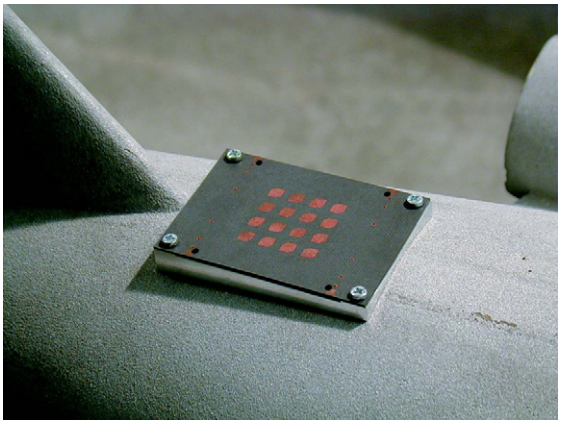

Fig. 10. Antenna array mounted on the Fokker 100 scaled model.

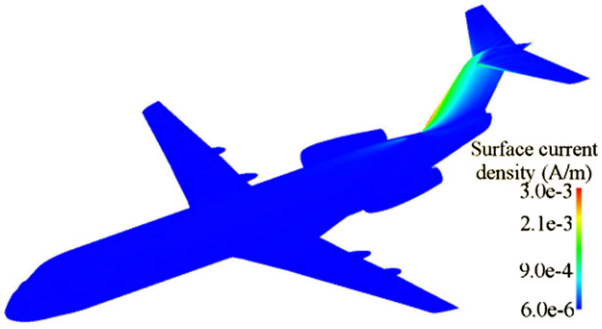

Fig. 11. Surface current density on the Fokker 100 scaled model simulated with the SB array pointing the main beam rearwards.

5. Measurement setup

Since the microstrip arrays described in Section 3 present a relatively high directivity, and considering that the electrical dimensions of the mock-ups are very large, it has been verified that the airframes have a very low influence on the installed performance depending on where the antenna is positioned. For this reason, a good validation of numerical predictions should be performed in a situation where the airframe really modifies the radiation characteristics of the antenna. Using the arrays described in Section 3, this is achieved if they are placed nearby a "critical position", which means a place close to possible sources of reflections. For these reasons, the position chosen to install the arrays is located close to the tails of both scaled models.

An adaptation of the mock-ups was necessary to install the antennas. In Fig. 8, the hole cut in the Fokker 100 model is shown in detail. This was needed because the feed networks of the arrays were open at the bottom and no ground plane exists below the feed lines in the stack up shown in Fig. 1(a). The planar shape of the antennas was adapted to the curved surface of the fuselages using metallic supports depicted in Fig. 9. It was designed so that it also connects electrically the ground plane of the antenna to the surface of the models. Finally, Fig. 10 shows one microstrip array installed on the Fokker 100 scaled mock-up. A similar procedure has been used for the IPAS-1 model.

The far-field measurements have been undertaken in DLR's outdoor range, where the antenna installed on the models was operating in receiving mode. The minimum distance d needed between the transmitter antenna and the mock-ups in order to satisfy the far-field condition is given by [2]

$$d > \frac{2D^2}{\lambda_0}, \tag{1}$$

where D is the larger dimension of the aperture representing the device under test (DUT) and λ_0 is the wavelength in free space. If the length of the Fokker 100 model is taken as D, then a minimum distance d of approximately 810 m would be needed for tests at 22 GHz.

Due to the large electrical dimensions of the mock-ups and due to the directive radiation patterns of the arrays, it is expected that the current densities induced on the aircraft surfaces may be strong only in the locations near to the installed array. Consequently, one could consider that the effective aperture diameter D is smaller than the complete length of the airframes. This supposition can be confirmed by looking at the currents induced on the surface of the Fokker 100 model computed using the MLFMM as shown in Fig. 11. The calculations were made considering the SB array installed close to the tail. One can see that the currents are not significant in most of the airframe in comparison to the intensity induced on the tail. For this reason, it is expected that the consideration of a dimension D smaller than the length of the airframe would not have much impact on the measurement accuracy. Considering that the distance between the two towers of DLR's measurement facility is 220 m, a DUT with an equivalent maximum aperture dimension $D = 1.22$ m could be measured accurately. After an analysis of Fig. 11, these values were considered acceptable and, therefore, used during the measurements.

Pictures of the measurement setup are shown in Fig. 12, where the tower holding the Fokker 100 model can be seen, and in Fig. 13, where the tower holding the transmitting antenna is presented. This last picture has been taken from the base of the tower holding the mock-up, where a pyramidal horn antenna has been installed. The signal received by this antenna was used as the

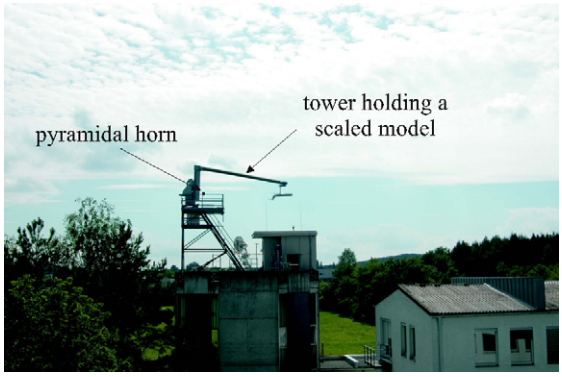

Fig. 12. Far-field measurement setup.

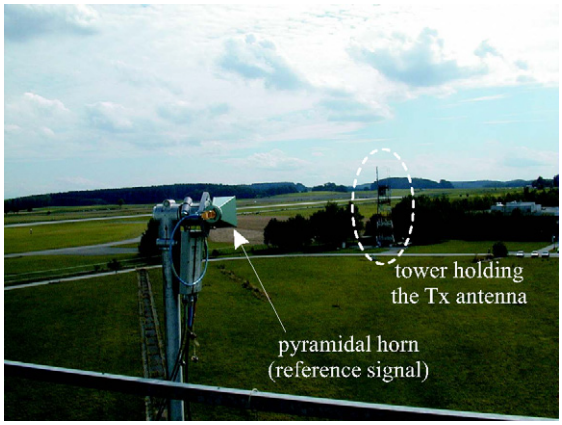

Fig. 13. Photo taken from the measurement tower showing the pyramidal horn used to receive the reference signal and the tower where the transmitting antenna was installed.

Fig. 14. Fokker 100 scaled model installed on the measurement tower.

reference signal to compensate undesired power fluctuations that may occur during the measurements.

Photos of the models installed on the measurement tower of DLR's antenna measurement facility are shown in Figs. 14 and 15.

6. Comparison between numerical and experimental results

6.1. Results for the Fokker 100 scaled model

The resulting radiation patterns of the BD array installed on the Fokker 100 scaled mock-up are shown in Figs. 16 and 17, where measured and computed results are compared in the pitch and roll planes. Very good agreement is obtained for both RHCP and LHCP.

Fig. 15. IPAS-1 model installed on the measurement tower.

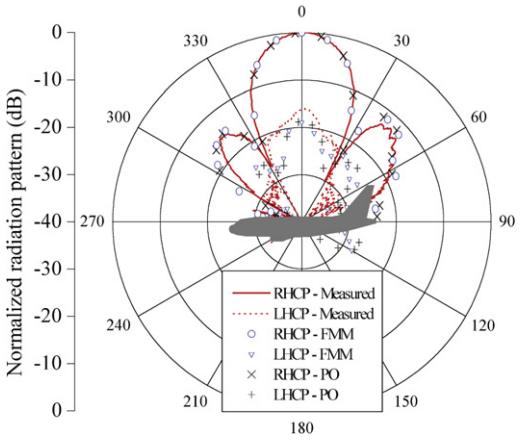

Fig. 16. Comparison between measured and computed results in the pitch plane with the BD antenna installed on the Fokker 100 scaled model.

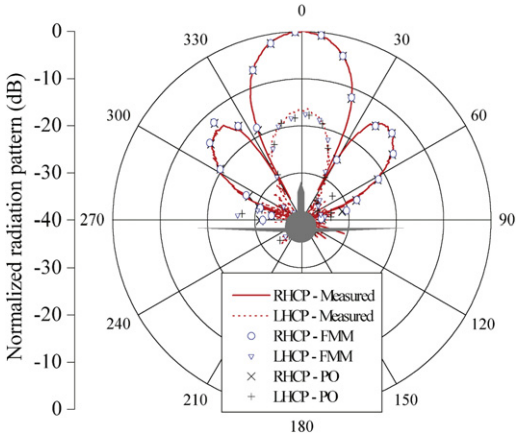

Fig. 17. Comparison between measured and computed results in the roll plane with the BD antenna installed on the Fokker 100 scaled model.

Fig. 18 shows the radiation pattern for the case of installing the SB array on the Fokker 100 model so that the main beam points to the front of the aircraft. Good agreement between simulated and measured results can be seen for both polarizations. The second analysis was performed by considering the case where the main beam points rearwards. This means that the tail of the aircraft is illuminated. The computed and measured radiation patterns are presented in Fig. 19. Whereas very good agreement was obtained in terms of co-polarization, some discrepancies can be observed for the cross-polarization in the region of the main lobe (around

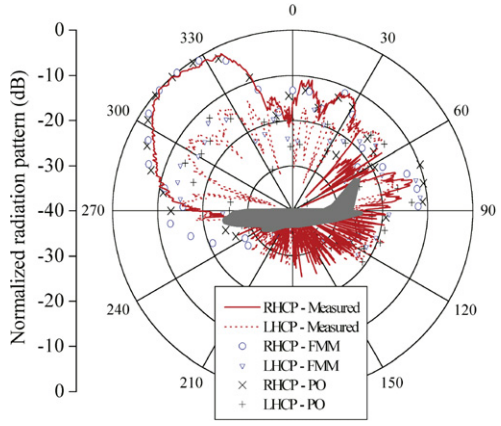

Fig. 18. Comparison between measured and computed results in the pitch plane with the SB antenna installed on the Fokker 100 scaled model. The main beam points forwards.

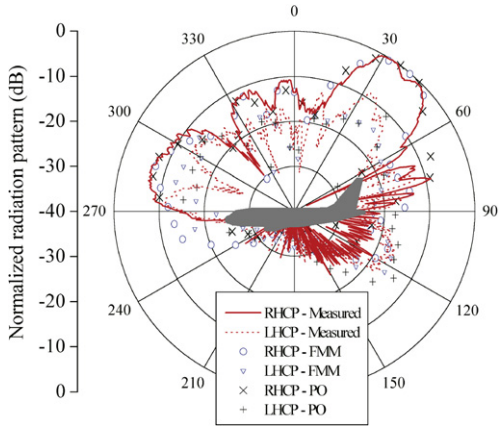

Fig. 19. Comparison between measured and computed results in the pitch plane with the SB antenna installed on the Fokker 100 scaled model. The main beam points rearwards.

$\theta = 30°$). For directions nearby $\theta = 120°$, the effect of the reflections from the horizontal stabilizer can be seen. The level of the LHCP component is higher than the co-polarization for both the measured and the computed results in this region. Also, the level of LHCP nearby $\theta = 120°$ is stronger in Fig. 19 than in Fig. 18, because the horizontal stabilizer is illuminated by the main beam in the former graphics and only by a side lobe in the latter one.

Looking from the bottom part of the tail, the currents computed with MLFMM and PO are shown in Fig. 20. The influence of multiple reflections, forming a standing wave profile on the current distribution, can be clearly seen in the calculations with MLFMM. With this method, the currents also vary smoothly, in contrast with the ones computed with PO. With this last approach, an abrupt transition between the illuminated and shadow areas can be observed.

Although the antenna has been installed quite near to the tail, the agreement between computations and measurement is good. The accuracy in the predictions of the LHCP component could be further improved, if the complete geometry could have been included in the electromagnetic simulations. For the reasons discussed in Section 2, this could not be done with the current available computational power.

6.2. Results for the IPAS-1 model

The computations for the IPAS-1 model have been carried out only employing the PO technique, since the available computational resources were not sufficient to simulate the problem with the MLFMM.

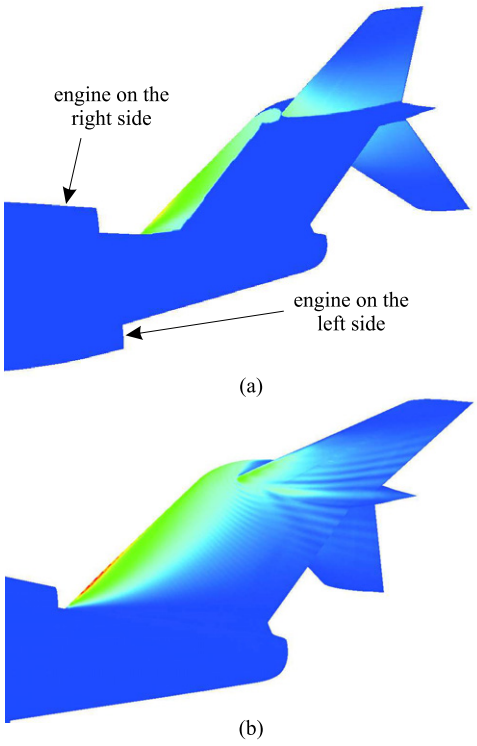

Fig. 20. Bottom view of the Fokker 100 tail (viewed from the right to the left). Current densities computed with (a) PO; (b) MLFMM.

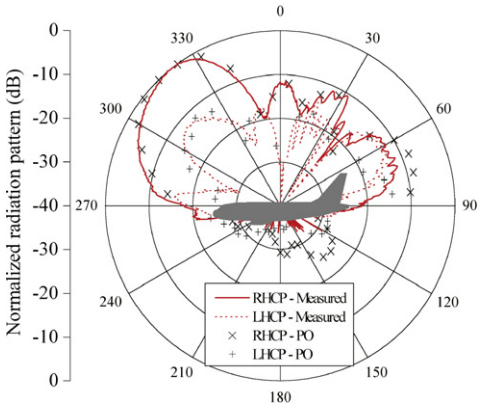

Fig. 21. Comparison between measured and computed results in the pitch plane with the SB antenna installed on the IPAS-1 model. The main beam points forwards.

The resulting radiation patterns with the SB array installed so that its main beam points forewards is shown in Fig. 21, where measured and computed results are compared. Good agreement can be seen for both polarizations. By rotating the SB antenna around 180°, the radiation patterns obtained are presented in Fig. 22. Good agreement is obtained between the measured and computed results for the main polarization. Some differences can be observed for the LHCP component. It is interesting to notice that for directions nearby $\theta = 120°$, no strong cross-polarized field exists (both in the computations and measurements), in contrast with the results obtained with the Fokker 100 model. The reason is that the horizontal stabilizer of the IPAS-1 model is not directly illuminated, since it is located in a shadow region related to the microstrip array.

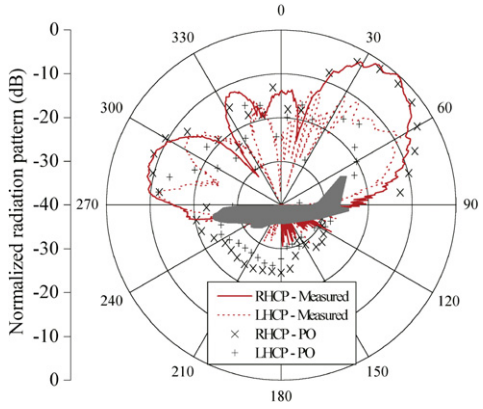

Fig. 22. Comparison between measured and computed results in the pitch plane with the SB antenna installed on the IPAS-1 model. The main beam points rearwards.

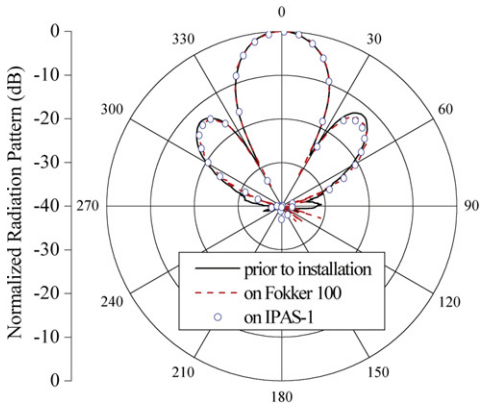

Fig. 23. Measured results in the roll plane before and after the installation of the BD array on the mock-ups.

7. Influence of the airframes on the radiation pattern of the arrays

In the last section, the installed performance of the arrays on different aircraft was shown separately. In this section, the main focus is to assess how much each of the mock-ups modifies the original radiation pattern, i.e. prior to the installation of the arrays.

The radiation patterns for the BD array in the roll and pitch planes are shown in Figs. 23 and 24. No strong changes can be observed by comparing the results before and after the installation. By examining the results in the pitch plane, one can see that only small discrepancies occur and only in the regions of the sidelobes, although both the mock-ups considered are very different in terms of shape, especially in terms of vertical and horizontal stabilizers.

In the case of the SB array, stronger deviations can be observed as shown in Fig. 25. Considering the array radiating with the main lobe pointed to the front of the mock-ups, stronger radiation can be seen in the angular ranges of $90° < \theta < 120°$ and $240° < \theta < 270°$ for the pattern of the array in free space due to shadowing caused by the airframes after antenna installation. The main discrepancies in the patterns are in the rear part, where the influence of the stabilizers can be seen mainly for the case of installation on the Fokker 100 mock-up. Nevertheless, despite the different tail geometries of both aircraft, the patterns are not strongly affected in the region of the main lobe.

Finally, by rotating the SB array 180° related to the previous case, the measured results are shown in Fig. 26. The main lobe illuminates directly the stabilizers now. Consequently, a null is obtained for the case of installation on the Fokker 100 mock-up in the region where originally the main beam would be located.

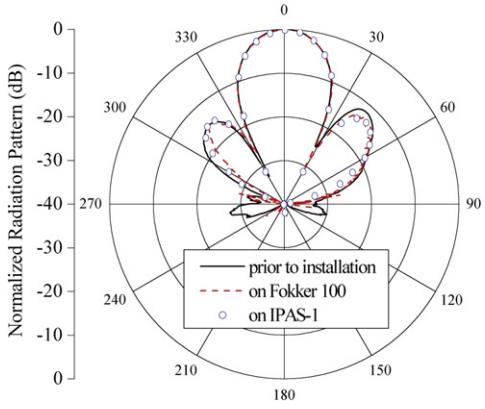

Fig. 24. Measured results in the pitch plane before and after the installation of the BD array on the mock-ups.

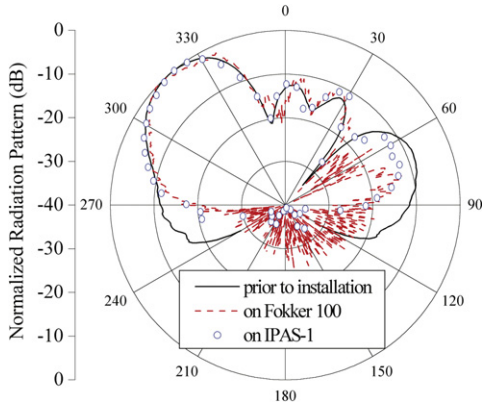

Fig. 25. Measured results in the pitch plane before and after the installation of the SB array on the mock-ups with the main beam pointing to the front of the aircraft.

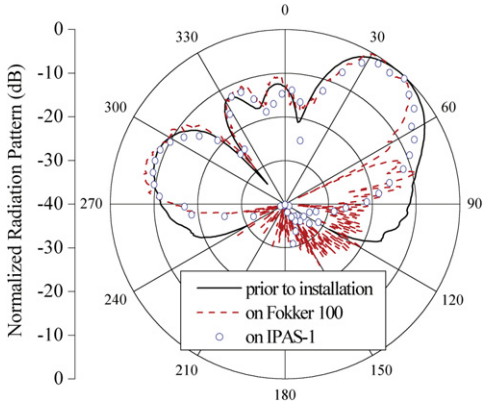

Fig. 26. Measured results in the pitch plane before and after the installation of the SB array on the mock-ups with the main beam pointing rearwards.

Moreover, the resulting main lobe gets narrower due to this fact. In the case of the IPAS-1 model, the shape of the main beam does not seem to be changed strongly related to the original pattern prior to the installation, although the main beam is pointing directly to the vertical stabilizer.

8. Conclusion

In this paper, the installed performance of microstrip antenna arrays on different passenger aircraft has been assessed. A simulation procedure that trades off computational needs and accuracy has been described. Validation of the simulations has been carried out experimentally by using scaled mock-ups. In the cases

presented in this contribution, the radiation characteristics could be in general well predicted by the simulations, although an antenna defeatured model and larger mesh elements than it is usually recommended have been used in the computations.

Strong influence could be observed only for the case of the SB array when the main beam points directly to reflecting surfaces and for the Fokker 100 model, where the stabilizers are mounted above the fuselage and thus illuminated by the antenna. For the IPAS-1 mock-up, no severe pattern degradation was observed even when the main beam was pointing directly to the vertical stabilizer. Although the arrays were positioned quite close to the tail in our experiments, no strong distortion of the patterns has been observed for the cases where the main beam does not illuminate the stabilizers directly.

The main reasons for some inaccuracies that were observed are attributed to the fact that the geometry of the microstrip arrays were not included in the simulations. Moreover, the use of the PO technique is more efficient if the source is located electrically far away from the scatterer. Furthermore, this technique yields more accurate results if the waves impinge upon the reflecting surfaces with nearly normal incidence. In the cases considered in this paper, these two conditions were not completely fulfilled in the surfaces of the tails of both Fokker 100 and IPAS-1 models. Nevertheless, the computed results are in rather good agreement with the measured radiation patterns.

Better agreement between computations and measurements would have been obtained if the complete geometry of the antenna, including all the dielectric layers, could have been included in the simulations. At present, this is still a difficult task. The fast increase in the computational power and the improvement on the numerical methods in Electromagnetics will surely make this possible in the future.

Acknowledgements

The authors would like to thank the Dutch National Aerospace Laboratory (NLR) and EADS Innovation Works (Toulouse, France) for providing us with the CAD models and the scaled mock-ups, so that we could perform the computations and the measurements at the DLR's antenna measurement facility. This work has been performed in the IPAS project, which was co-funded by the European Commission within the 6th Framework Programme (2002–2007) under Contract ref: AST3-CT2003-503611.

References

[1] Ansoft Designer User's Manual, Ansoft Corporation, 2008.
[2] C.A. Balanis, Antenna Theory: Analysis and Design, 2nd ed., John Wiley & Sons, New York, 1997.
[3] A. Barka, Assessment of spectral basis functions in BEM/FEM/GSM domain decomposition methods for scattering and radiation applications, in: IEEE Int. Symp. on Antennas Propagat., San Diego, CA, USA, 2008.
[4] A. Barka, P. Caudrillier, Multidomain electromagnetic modelling for installed performance of antennas on aerostructures (IPAS), in: IEEE Int. Symp. on Antennas Propagat., Washington, DC, USA, 2005.
[5] A. Barka, P. Caudrillier, Domain decomposition method based on generalized scattering matrix for installed performance of antennas on aircraft, IEEE Trans. Antennas Propagat. 55 (6) (2007) 1833–1842.
[6] B. Bencivenga, F. Mioc, L.J. Foged, M. Sabbadini, S. Filippone, E. di Giampaolo, Computationally efficient tool using UTD on detailed meshed geometries, in: IEEE Int. Symp. on Antennas Propagat., Charleston, SC, USA, 2009.
[7] M. Cuntz, A. Konovaltsev, A. Hornbostel, E. Schittler-Neves, A. Dreher, GALANT – Galileo antenna and receiver demonstrator for safety-critical applications, in: Proceedings of the 10th European Conf. Wireless Technology, Munich, Germany, 2007, pp. 59–61.
[8] FEKO User's Manual, EM Software & Systems – S.A. (Pty) Ltd, 2005.
[9] M.V.T. Heckler, A. Dreher, Analysis of monopoles installed on airframes, in: IEEE Int. Symp. on Antennas Propagat., Washington, DC, USA, 2005.
[10] M.V.T. Heckler, A. Dreher, Comparison of asymptotic and full-wave predictions of installed antenna performance on airframes, in: Proceedings of the German Aerospace Congress 2006, Braunschweig, Germany, 2006, pp. 49–54.
[11] M.V.T. Heckler, A. Dreher, Analysis of planar 4×4 microstrip antenna arrays installed on airframes, in: 2nd European Conference on Antennas and Propagation, Edinburgh, UK, 2007.
[12] IPAS Project Proposal, Annex 1 – Description of Work FP6-2002-Aero-1-503611, contract no. AST3-CT-2003-503611, 2003.
[13] T.M. Macnamara, Introduction to Antenna Placement & Installation, John Wiley & Sons, London, 2010.
[14] A. Thain, D. Clerc, S. Fredj, S. Gerbal, Calculated and measured in-flight antenna patterns on an ATR 72 aircraft, in: 2nd European Conference on Antennas and Propagation, Edinburgh, UK, 2007.
[15] A. Thain, G. Peres, J.-P. Estienne, G. Sylvand, P. Cailleu, P. Benjamin, I. Terrasse, G.-P. Piau, G. Sabanowski, Numerical modelling of aircraft antenna installations, in: 2nd European Conference on Antennas and Propagation, Edinburgh, UK, 2007.
[16] Ç. Tokgöz, C.J. Reddy, R.J. Burkholder, P.H. Pathak, Application of UTD for prediction of radiation pattern and mutual coupling associated with antennas on faceted airborne platforms, in: IEEE Int. Symp. on Antennas Propagat., Charleston, SC, USA, 2009.